Geophys. J. Int. (1993) **112,** 344–358

2-D tomographic imaging across the North American Mid-continent Rift System

D. A. Hamilton and R. F. Mereu

Department of Geophysics, University of Western Ontario, London, Ontario N6A 5B7, *Canada*

Accepted 1992 July 30. Received 1992 July 1; in original form 1991 December 15

SUMMARY

2-D traveltime tomography was used to model the seismic-velocity structure of the Mid-Continent Rift System underneath Lake Superior. The data set came from Line A of the 1986 Great Lakes International Multidisciplinary Program on Crustal Evolution (GLIMPCE) experiment. In-line data analysed in this study were recorded on four land stations and on five ocean-bottom seismometers. Shot spacing on the 240 km long line was approximately 333 m. Both direct and refraction arrival times were used to image the upper crust before expanding the process to cover greater distances and depths. Crustal thickness was determined using reflection (*PmP*) data from the Moho. Several known near-surface structures were resolved. An extensive high-velocity zone (7.0–7.2 kms^{-1}) under the central basin of the lake was found to be composed of a plume-like structure rising to a depth of approximately 10 km. This plume originates from a broader-based (approximately 50 km) mantle bulge, and probably indicates an area of crustal weakness along the rift. A smaller, less complex intrusion appears under the northern basin of the lake. Moho depths increase from about 36 km under the southern flank to about 55 km under the central basin, decreasing again to about 45 km in the north. There is some evidence in the *PmP* seismic record that the Moho under the central basin is a disrupted transition zone. The velocity model presented here corroborates this. A stability test applied to the tomography velocity model—along with comparisons to other Line A models—indicate that the result is a reliable and a reasonable representation of the Mid-continent Rift System under Lake Superior. These findings support the theory that this complex structure is part of a failed Keweenawan (1100 Ma) tectonic rifting event.

Key words: GLIMPCE, Mid-Continent Rift, seismic inversion, tomography.

INTRODUCTION

In this paper, we present a detailed velocity model of the 1986 GLIMPCE experiment Line A data set across the North American Mid-continent Rift System using a 2-D seismic tomography inversion technique.

It is generally accepted that Lake Superior lies along a 1.1 billion-year-old failed continental rift, known as the Mid-Continent Rift System (MRS). The MRS is approximately 2000 km long, running from central Kansas to Lake Superior where it hooks SE through Michigan. It is characterized in part by the presence of gravity and magnetic anomalies (Van Schmus & Hinze 1985). The cause of these anomalies is believed to be massive mantle-derived material—namely basalt—that has intruded and has been deposited in the rift zone (Steinhart & Smith 1966; Luetgert & Meyer 1982). The crust under Lake Superior is considered to be a graben-like structure filled with mafic volcanics and clastic sedimentary rocks (Hinze, Wold & O'Hara 1982; Klasner, Cannon & Van Schmus 1982). Seismic data from the 1963 Lake Superior experiment suggest a crust exceeding 50 km depth under the central basin, yet of variable thickness elsewhere (Berry & West 1966). This has been verified by Behrendt *et al.* (1988), Cannon *et al.* (1989), Epili & Mereu (1989); by Tréhu *et al.* (1991).

The Lake Superior Basin is part of the Southern (geological) Province of the Canadian Shield, and is the only area that contains exposures of Keweenawan age (1100 Ma) volcanics (Hinze & Wold 1982). This Keweenawan sequence

forms a large syncline incorporating much of Lake Superior, and has been associated with economic mineral deposits. The importance of the MRS today lies primarily in studies of the tectonics responsible for its appearance.

The 1986 Great Lakes International Multi-disciplinary Program on Crustal Evolution (GLIMPCE) Experiment comprised both extensive seismic refraction and wide-angle reflection surveys in the vicinity of the Mid-Continent Rift. Participants in this experiment included the Geological Survey of Canada (GSC), the United States Geological Survey (USGS) and several academic institutions. In the GLIMPCE Experiment, three lines A, B, and C were shot perpendicular to the MRS. In this paper, we chose to use only the data from Line A (Fig. 1) as this was the only line that had enough in-line stations (ocean-bottom seismometers) to perform an adequate tomography modelling study. The five ocean-bottom seismometers (OBSs) on the floor of Lake Superior, the land stations at the ends of the line, and the shot spacing of approximately 333 m, allowed for good coverage of the area. A model of the upper crust along Line A constructed by the GLIMPCE Seismic Refraction Working Group (1989) showed high velocities (7.0 km s^{-1})) at relatively shallow depths (12 km), suggesting intrusions of mantle material. A detailed whole-crust Line A model by Tréhu *et al.* (1991) confirmed this modelled intrusion, and displayed a disrupted Moho. These results were based on iterative, forward-modelling trial and error methods.

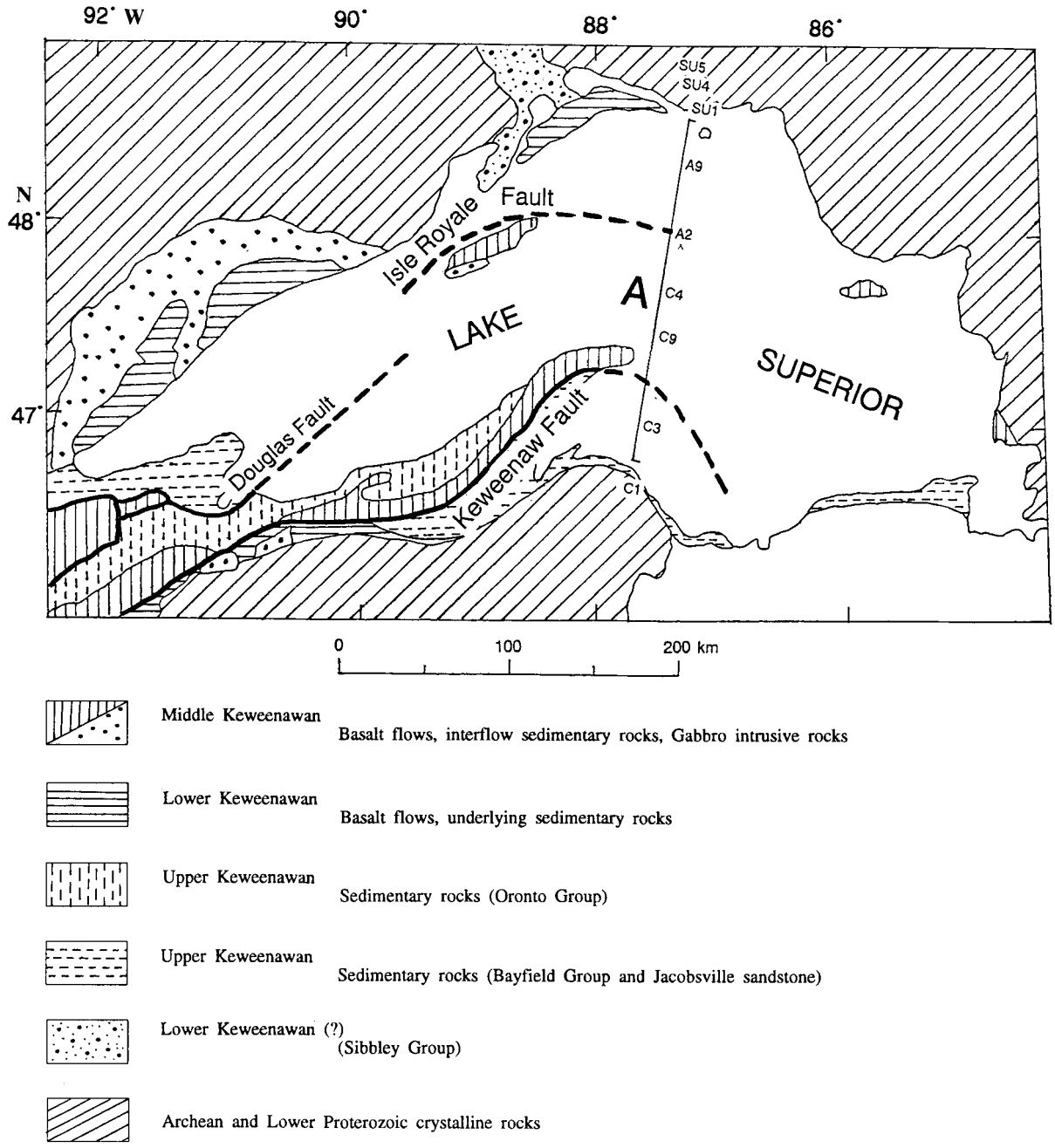

Figure 1. Line A and seismic station locations in Lake Superior. Geological interpretation after Cannon & Davidson (1982).

Because of the trace spacing used in this experiment, these Line A data were well suited for application in a 2-D traveltime tomographic inversion method. In this paper we are presenting an alternative modelling method for the GLIMPCE Line A data set based on traveltime tomography. This reduces the amount of inherent subjectivity associated with trial and error techniques and leads to a more reliable model (White & Boland 1992).

The traditional problem in seismic tomography is to reconstruct an image of the velocity structure of the Earth, or some portion thereof. Velocities cannot be measured directly; however, traveltimes of the seismic waves as they move from a source to a detector can be measured. Knowing these traveltimes and estimating the distance that these waves travelled, it is then possible to estimate the velocity at which they moved. This is accomplished by discretizing a model into cell blocks and solving for their constituent velocity gradients by inversion of the traveltimes.

Cross-borehole tomography studies employ straight ray path approximations for the propagating waves (Peterson, Paulson & McEvilly 1985; Bregman, Bailey & Chapman 1989); however, in surface-to-surface refraction experiments such as this one, curved ray path modelling is essential because of the greater distances and depths involved. Dines & Lytle (1979), Bishop *et al.* (1985), and Bording *et al.* (1987) present excellent discussions of both short- and long-distance tomographic studies.

Difficulties using tomographic methods with exploration seismic arrays include severe geometrical limitations and a general lack of data for the kind of redundancy that is desired. Geometrical limitations can be overcome somewhat by considering earthquake data. Aki, Christoffersson & Husebye (1977) used *P*-wave arrival times to determine 3-D structure of the lithosphere. Dziewonski & Anderson (1984) did this to model the Earth's mantle, and Beghoul, Hearn & Barazangi (1991) used *Pn* data from earthquakes to image the western United States. For in-line explosion seismology modelling, images can be distorted by edge effects, by cell size, and especially by the number of rays travelling through a given cell. Careful selections of initial model parameters are necessary to help improve the reliability of the results. Nolet (1987) has edited a volume on the entire subject, including various seismic tomography inversion methods. The technique employed in this paper follows closely that of White (1989).

GLIMPCE LINE A DATA

The Line A survey utilized both land and ocean-bottom seismometers. Stations used in this study are shown in Fig. 1. The geological interpretation shown there is that presented by Cannon & Davidson (1982). The three north-shore stations were controlled by the GSC, and the University of Wisconsin operated the south shore station. The USGS were in charge of the five OBSs.

Traveltime data were generated from a total of 640 marine air-gun blasts over a 22 hr period. Data from many of the other stations in the experiment were contaminated with noise. Survey details and a complete set of record sections are given by Morel-à-l'Huissier *et al.* (1990). Examples of recorded data for the C1 land station and for the SU5 land station are shown in Fig. 2(a) and (b).

The C1 record in Fig. 2(a) shows virtually noise-free first arrivals and sharp, clear *PmP* reflections from the Moho. Also visible in this record are the multiple and discontinuous intracrustal and *PmP*-reflection signals. Deconvolution attempts to improve the sections were not very successful (Epili & Mereu 1991). This observation is consistent with previous geophysical experimental results that suggest the possibility of a highly-disrupted Moho transition zone under the lake (Hinze, Wold & O'Hara 1982; Hinze & Wold 1982). Because *PmP* reflections have a short critical distance near C1, it is likely that the Moho boundary is sharp in this southern region. Similar sharpness is not visible in the northern SU5 station because of the noise in the data.

In all, 4936 first arrival and *PmP* traveltimes were used in this analysis. Because of the varying lake bathymetry, these times were corrected to a datum plane at the surface of the lake. Seismic ray paths were assumed to travel through the water at 1.44 kms^{-1} and through the near-surface Shield rock at 5.5–6.0 kms^{-1}. In general, the southern station records were quite clear; however, the northern station records were contaminated with much noise, and this resulted in some difficulty with traveltime picking from that part of the line. The picked data were weighted according to their reliability. For example, arrivals near a station were generally less contaminated with noise than those at great distance from the station. As such, the former data were given more weight (manually, based on amplitudes) in the inversion than were the latter.

MODELLING STRATEGY

After the arrival-time data were collected and weighted, the modelling process consisted of ray-trace forward modelling and tomographic inversion of the data.

Ray tracing

Ray tracing through a velocity model to observe the traveltimes associated with the medium plays an integral part in the subsequent data inversions because comparisons are needed between theoretical and observed times. A highly-useful ray-tracing technique is the triangular block model method described by Mereu (1990). In this method, an initial velocity model is constructed such that velocity variations with depth and with horizontal distances may be used.

A model is discretized into triangular cells and each cell contains its own 2-D linear-velocity function

$$V(x, z) = ax + bz + c, \tag{1}$$

where $V(x, z)$ is the seismic velocity at any point (x, z) in the model, and the constants a, b and c are determined from the velocity values assigned to each vertex (node) of every triangle. These constants will normally differ from cell to cell.

Initializing the model in this manner yields a constant velocity gradient of the form

$$\mathrm{Grad}\, V = a\mathbf{i} + b\mathbf{k} \tag{2}$$

in each cell ($\mathbf{i}$ and $\mathbf{k}$ are unit vectors in the x and z directions

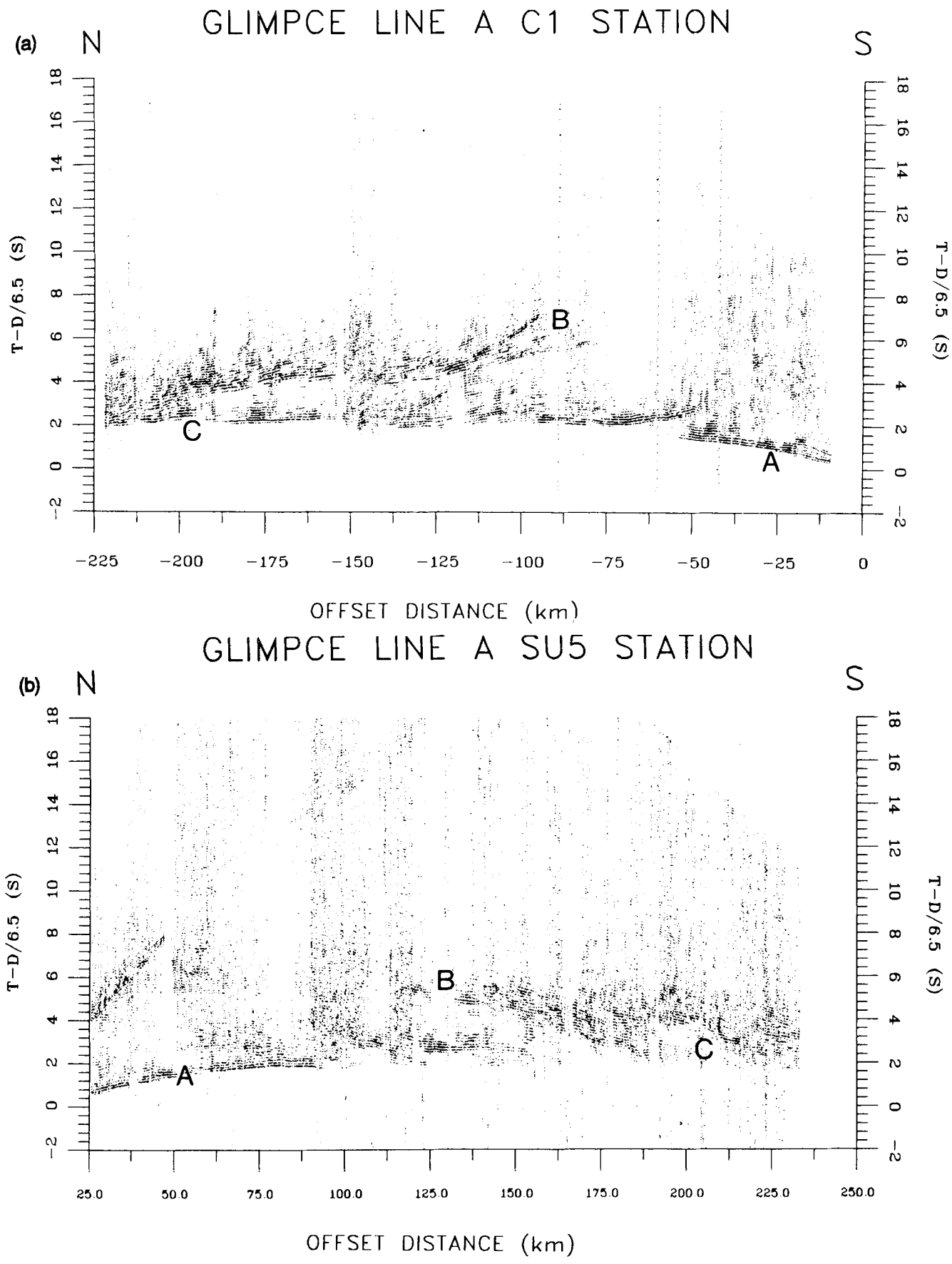

Figure 2. Seismic record sections from the southern land station C1 (a) and the northern land station SU5 (b). In both sections, **A** = near-shot refraction signals, **B** = reflection (*PmP*) signals, and **C** = large offset refraction signals. In (a), both near and far refraction signals are virtually noise free, and multiple reflection branches from the Moho are evident. In (b), the far away refraction signals and Moho reflections are contaminated with noise. Furthermore, the *PmP* signals appear to be discontinuous.

respectively). This ensures that all ray paths traced through the cells will be arcs of circles. The ray-tracing method itself solves these ray arc equations with boundary line equations (where applicable). Snell's law for rays propagating across an interface is applied at each intersection point. Velocity gradients are necessary when dealing with large offsets, as velocity generally increases linearly with depth in the Earth.

Triangles are chosen for the cell shapes because they minimize the number of cell parameters and are very effective in modelling dipping structures and/or faults.

Tomographic inversion procedure

The tomographic inversion method begins with a comparison of observed traveltimes and traveltimes derived from ray tracing. The differences between these are used to infer nodal velocity updates in each cell.

Before inversion takes place, a matrix **A** of partial traveltime derivatives is constructed such that the system of equations

$$\mathbf{Ax} = \mathbf{b} \tag{3}$$

is satisfied. Thus, A_{ij} is $\dfrac{\partial T_i}{\partial v_j}$, where ∂T_i is a traveltime perturbation from the ith ray observed when the jth nodal velocity ∂v_j is perturbed. The vector **b** represents the traveltime differences at each station ($t_{\text{observed}} - t_{\text{model}}$), and **x** is a vector of velocity perturbation solutions (ΔV).

Since the observations are weighted according to their uncertainty σ_j, the system of equations is multiplied by $\mathbf{Q} = \text{diag}\left\{\dfrac{1}{\sigma_j}\right\}$. The system is then solved iteratively for the perturbations at each cell node, and the velocity model is updated with these solutions each time. The updated model is also smoothed at the nodes so that nodal discontinuities do not create false boundaries for the ray-tracing program. (Note that velocity is the model parameter used in this example, but nodal depths may be used equally well.) Mathematical details of this method are given by White (1989) and by Hamilton (1991).

The entire process is stopped once the differences between the observed and the model times are in the neighbourhood of the expected overall uncertainty. The total RMS traveltime misfit was used as a stopping criterion for the inversion process here, but presentation of the misfit should be standardized. As a result, the total RMS value for each model was divided by the number of rays traced (i.e. data points). These normalized RMS–ray values can then be compared quite easily. The drawback to this error presentation is that a few poorly-fitting data points will obviously affect the entire RMS–ray misfit value. Therefore, the visual fit of the theoretical and observed traveltimes is routinely checked in this method in order to identify and remove—if necessary—these outliers.

The inversion algorithm used here is singular value decomposition (SVD) based on the routine given by Press *et al.* (1986). SVD does not work well for large sparse matrices typical of seismic tomography problems (Scales 1987), but with a reasonable choice of model parameters—initial velocities, for example—we were able to apply it here successfully.

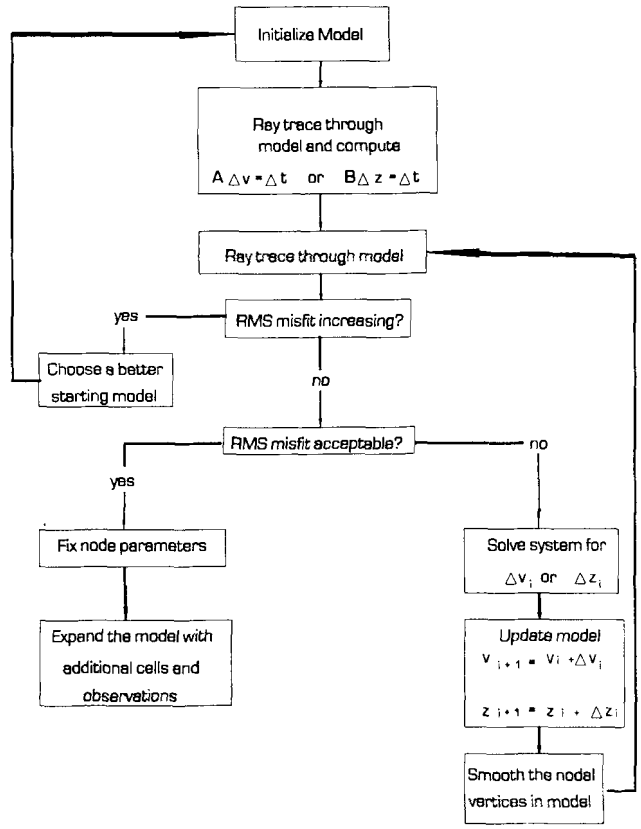

Figure 3. Flowchart showing the tomography technique used in this work. The method is used for both velocities (V_i) and Moho depths (Z_i). Monitoring the RMS misfit between model and observed traveltimes helps control the process. The inversion algorithm used in this paper was an iterative singular value decomposition technique.

To compensate for the sparseness of the **A** matrices, we computed solutions of velocity structure near the stations in the upper crust first before expanding cell sizes and observations to include the deep crust. By doing so, we were able to use SVD to arrive at reasonable velocities in a relatively short time. A flowchart of the inversion method used here is shown in Fig. 3.

Station separation distances across Lake Superior vary from about 28 km to around 55 km, allowing for upper crust modelling to depths of approximately 10–15 km. The structures between adjacent stations were derived first by using data from both the forward and reverse side. This coverage allowed for resolution of lateral velocity changes as well as for those associated with depth.

Initial model

The Line A area of Lake Superior was divided up into three submodels: the upper crust (0–15 km depth), the mid-crust (15–35 km depth), and the deep crust (35–55 km depth).

In the initialization of the submodels, horizontal cell sizes were chosen to be at least several times greater than the trace spacing. Cell depths were generally less than the horizontal dimensions since vertical resolution is normally greater than lateral resolution in surface-to-surface refraction modelling (White 1989). As the tomographic technique

was applied to deeper crustal regions, the cell sizes increased so that the number of rays travelling through these deep cells would always be similar to those travelling through any given near-surface cell. Naturally, the overall resolution of the images decreases at depth with expanding cell dimensions. The velocities chosen for the initial models were based on earlier Line A findings, primarily those of Epili & Mereu (1989) who used iterative forward-modelling methods on the data.

By considering the observed traveltime curves, areas of structural importance along the profile were identified. Cell placement and dimensions for these parts of the model were chosen to reflect the nature of the structural changes. This type of geological information is desirable to help constrain the inversion process.

Because ray coverage and first arrivals in the upper crust were very good, the resulting velocity structure for this area was fixed before expanding the inversion process into deeper crustal regions. A summary of the stations and station pairs, number of rays, and RMS–ray misfits for the entire model are presented in Table 1.

Table 1. Line A station pairs and individual stations used in the tomography modelling. The number of rays traced is also the number of observed data for the respective stations. The low RMS–ray misfits demonstrate the excellent fits achieved.

UPPER CRUST

Station Pairs		Number of Rays Traced	RMS/ray (msec)
C1	C3	73	5
C3	C1	86	6
C3	C9	82	2
C9	C3	148	3
C9	C4	76	5
C4	C9	79	5
C4	A2	107	6
A2	C4	108	10
A2	SU1	144	4
SU1	A2	81	3

MID-CRUST

Stations	Number of Rays Traced	RMS/ray (msec)
C1	239	6
C3	219	4
C9	72	2
C4	105	13
A2	223	3
A9	70	3
SU4	241	7
SU5	239	5

DEEP CRUST

Stations	Number of Rays Traced	RMS/ray (msec)
C1	489	23
C3	281	14
C9	138	31
C4	67	1
A2	124	7
A9	114	6
SU4	249	63
SU5	352	17

Upper crust inversion

Modelling of the shallow crust began at the southern end of Line A—using both direct and refracted wave data—and continued northward from there.

The first paired stations used in the inversion were C1 and C3, and the resulting velocity structure for the area between these two stations is shown in Fig. 4. It is clear that the region where the Pre-Cambrian Shield rock (PS) meets the Keweenawan sedimentary layer (KS) has been resolved around the 208 km mark. The rapid decrease in velocity near the C3 station is most likely due to the presence of the KS, whereas the higher velocities ($5.0\,kms^{-1}$–$6.0\,kms^{-1}$) are characteristic of Pre-Cambrian igneous and metamorphic rock.

This result is a smoothed velocity image. Velocity values returned from the inversion generally differ from cell to cell. A simple averaging of the values at nodes that are shared by at least two cells is performed to eliminate discontinuities at these points. As such, sharp boundaries between different velocity horizons are not present. In those areas where distinct boundaries in the upper crust were expected (based on geological evidence, for example), cell blocks of slightly differing velocity gradients were layered in order to simulate these structures.

Comparisons of observed and model times for this station pair along with the corresponding ray tracing diagram are shown in Fig. 5(a) and (b), and reveal very good fits. The velocity change from the KS to the Shield rock is evident in the OBS C3 station traveltime data, but is not visible for the C1 land station (Fig. 2a). This is due to the proximity of the C3 station to the velocity discontinuity.

Successive station pairs were analysed in the same manner until the entire profile had been covered. The resultant velocities of the upper crust were then considered to be fixed. Modelling of the mid-crust incorporated depths from 10 and 15 km to 35 km, and wide-angle refraction data only were used. Two areas of the mid-crust were defined using the C3–A2 and C1–SU4 station pairs. The former modelled down to a depth of 20 km and a lateral distance of 120 km, whereas the latter modelled to a depth of 20–35 km and a lateral distance of 233 km. A total of 19 cells were initialized for the C3–A2 pair, and 1408 traveltimes were inverted. For the C1–SU4 pair, 24 cells and 604 observations were used.

A ray-tracing diagram for all stations in the combined upper–mid crust modelling is presented in Fig. 6, and shows a maximum-refraction ray penetration of approximately

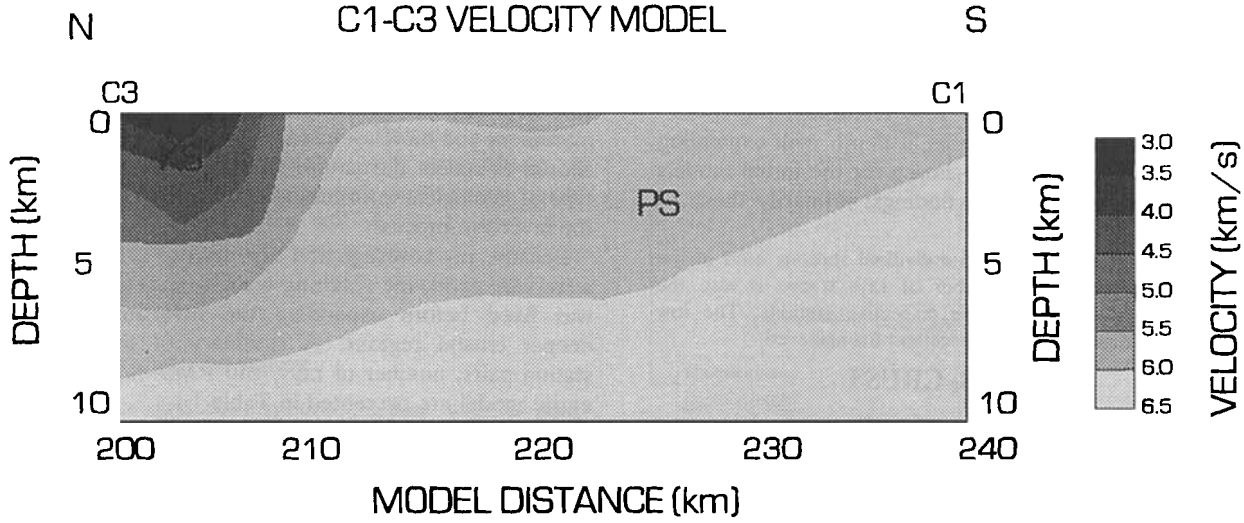

Figure 4. Velocity map of the upper crust between stations C1 and C3. Note the transition between the higher velocity Pre-Cambrian Shield rock (PS) and the lower velocity Keweenawan sedimentary layer (KS).

30 km depth. Only a representative number of rays have been traced here for clarity.

Deep crust inversion

The mid-crust model was fixed before we proceeded to image Moho depths. A total of 1814 rays were traced through an additional 15 cell blocks.

Modelling of the Moho depths was a little different from the previous shallow and mid-crust models. For instance, it is known that the Moho velocity in the Shield is approximately 8.1 kms^{-1} from *Pn* studies (Steinhart & Smith 1966). Also, the complete seismic records indicate that the Moho boundary near the C1 station is sharp,

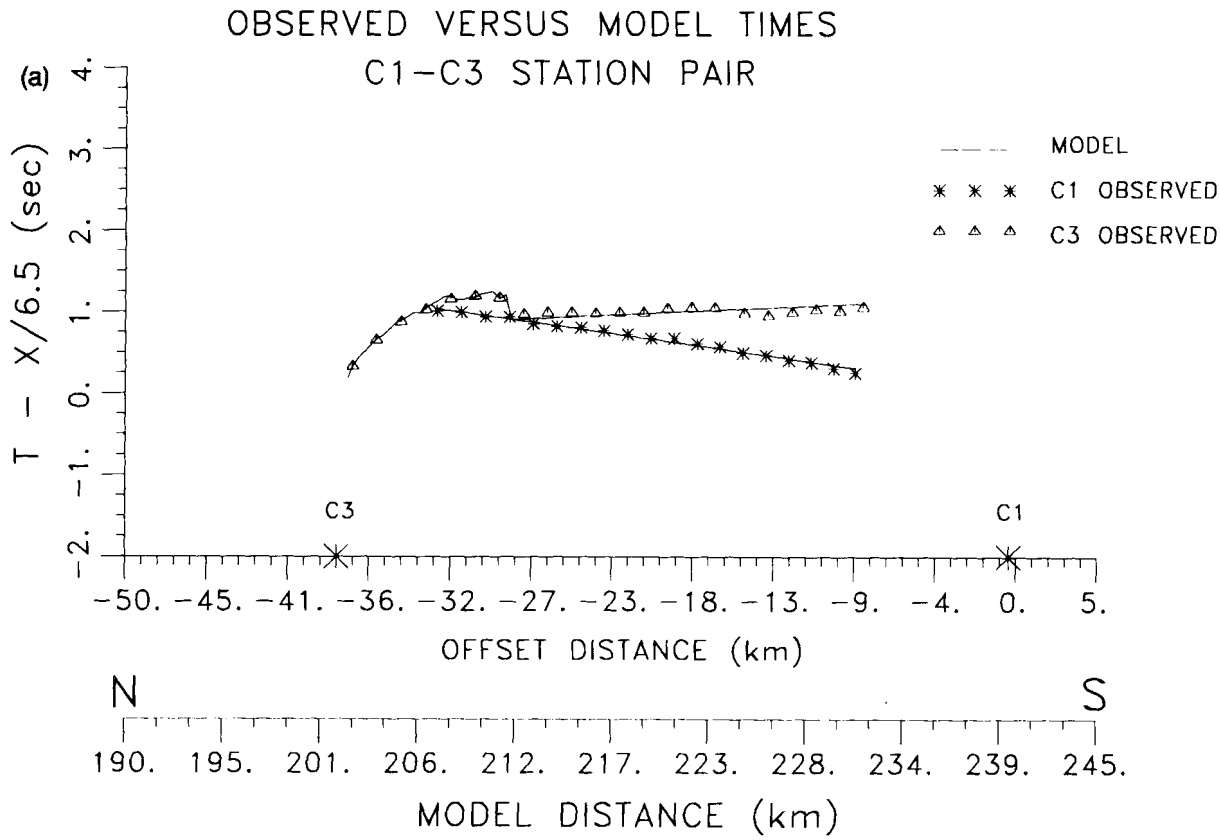

Figure 5. Traveltime comparisons between model and observed arrivals for the C1 and C3 stations (a) along with the ray-tracing diagram fo the same station pair (b). The complete upper crust was modelled using station pairs in order to help detect lateral velocity changes as well a those with depth. Upper crust velocities were then fixed before modelling greater distances and depths. (Not all times were plotted in (a) fo clarity.)

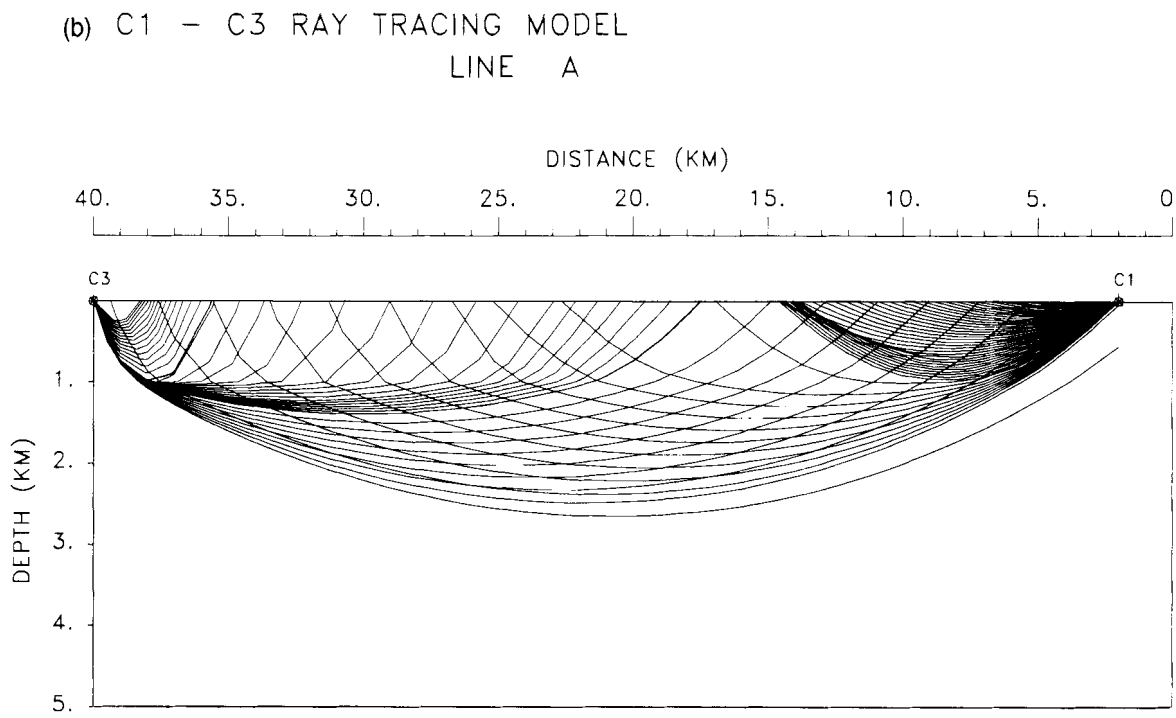

Figure 5 (b). (*Continued.*)

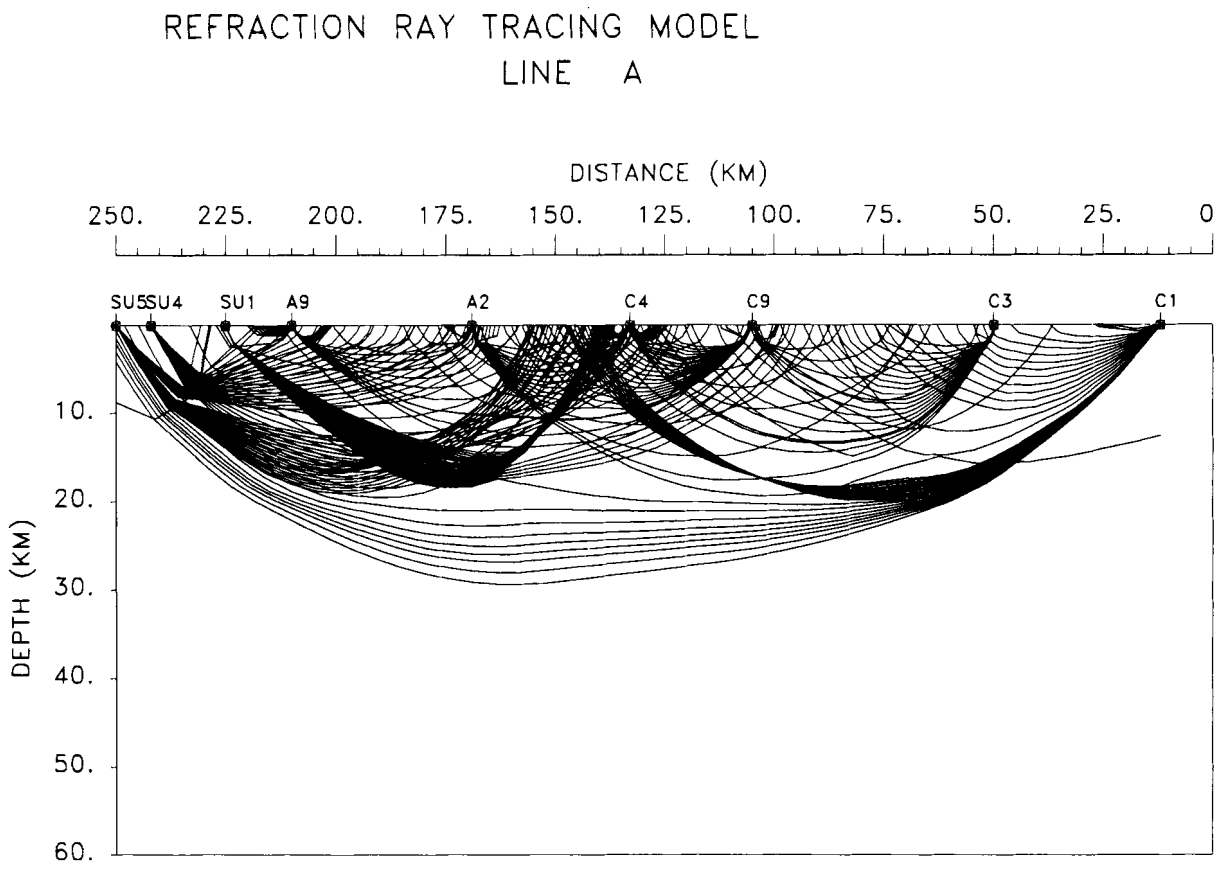

Figure 6. Upper–mid crust ray-tracing diagram for refraction data from all stations used in this work. Only a selected number of rays are displayed here for clarity.

whereas under the central basin of the lake, this boundary is unclear and discontinuous. This observation suggests that under the central basin, the Moho is transitional and highly disrupted. In picking the *PmP* arrival times, every effort was made to choose the main reflector branches. This was not always an easy task given the amount of noise and secondary branches present. As such, most of the data were given poor weights, and this means that the deep crust results are the least reliable of these tomography findings.

Since both velocities and horizon depths were unknown between depths of 35 km and the Moho boundary, these two parameters both had to be found. Based on the fact that the mid-crust velocities were considered fixed, the deeper cells were initialized with similar values. Moho depth estimates were taken from Epili & Mereu (1989). The C1 and SU1 *PmP* data were inverted first, and separately, to image better the Moho near those stations. No attempt was made to determine depths to better than $\pm 1\ \mathrm{km\,s^{-1}}$ as this would be unreasonable given the lack of geological information and of data reliability (compared to that of the upper crust).

Once the northern and southern Moho boundaries were placed, Moho depth under the central basin was considered. Late *PmP* arrival times from C3 indicate that the boundary is deeper in this area than it is at the edges of the lake. Furthermore, two main reflector branches observed in the C1 record (Fig. 2a) suggest at least two boundaries. As such, cell blocks under the central basin were initialized with rapidly increasing velocity gradients with depth in an attempt to model realistically this transition zone.

The general lack of *PmP* data from the northern stations made it difficult to initialize the northern basin. However, these records do possess several possible *PmP* branches and therefore, there is no evidence to suggest that the Moho transition zone defined in the central basin does not continue towards the north end of the lake.

With both the resolved and assumed boundary depths fixed, the overlying velocity structure was found in the same manner as were the upper- and mid-crust velocities. The resulting whole crust velocity model for the Line A profile is presented in Fig. 7.

A diagram of all the cells used in the whole crust modelling is shown in Fig. 8. A total of 157 cells were employed to image the crust under the Line A profile.

Stability test

Our line A model was compared with that of the GLIMPCE Seismic Refraction Working Group (1989) and that of Tréhu *et al.* (1991). General agreement exists for velocities in the upper–mid crust as well as for those of the intrusive material. The extent and geometry of the high-velocity zone in our model is somewhat different. In general, our model shows the up-welling in the Central Basin (150 km, 20 km) to be broader based and more complex than that depicted by Tréhu *et al.* (1991). The area where the Central Basin (CB) intrusion ends and the Northern Basin (NB) intrusion (75 km, 30 km) begins is less distinct in our model.

Our first concern was the reliability of our model. Lively discussions with our departmental colleagues led to the application of a stability test for this model. Because of the

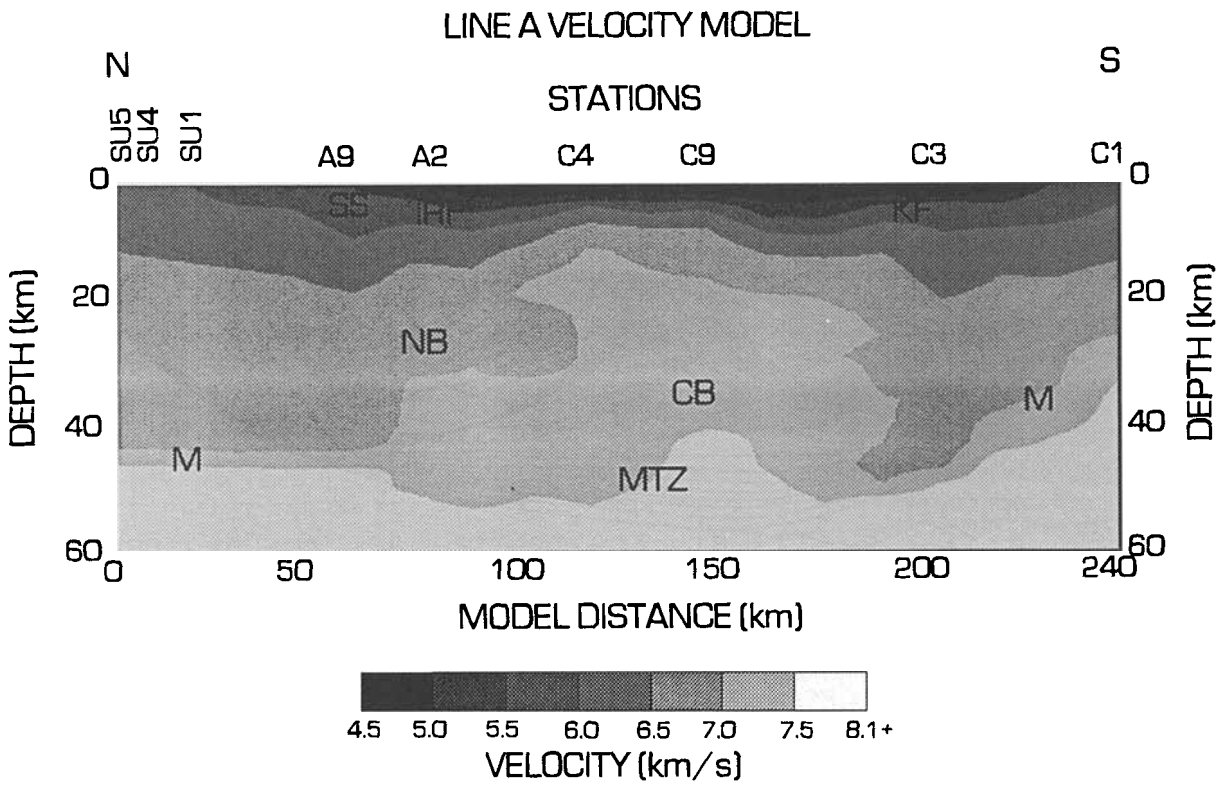

Figure 7. Velocity map of the whole crust under Line A. KF = Keweenawan Fault zone, IRF = Isle Royale Fault zone, SS = Superior Shoals, CB = Central Basin, NB = Northern Basin, M = Moho and MTZ = Moho Transition Zone. The mantle material intrusion is visible in the central basin.

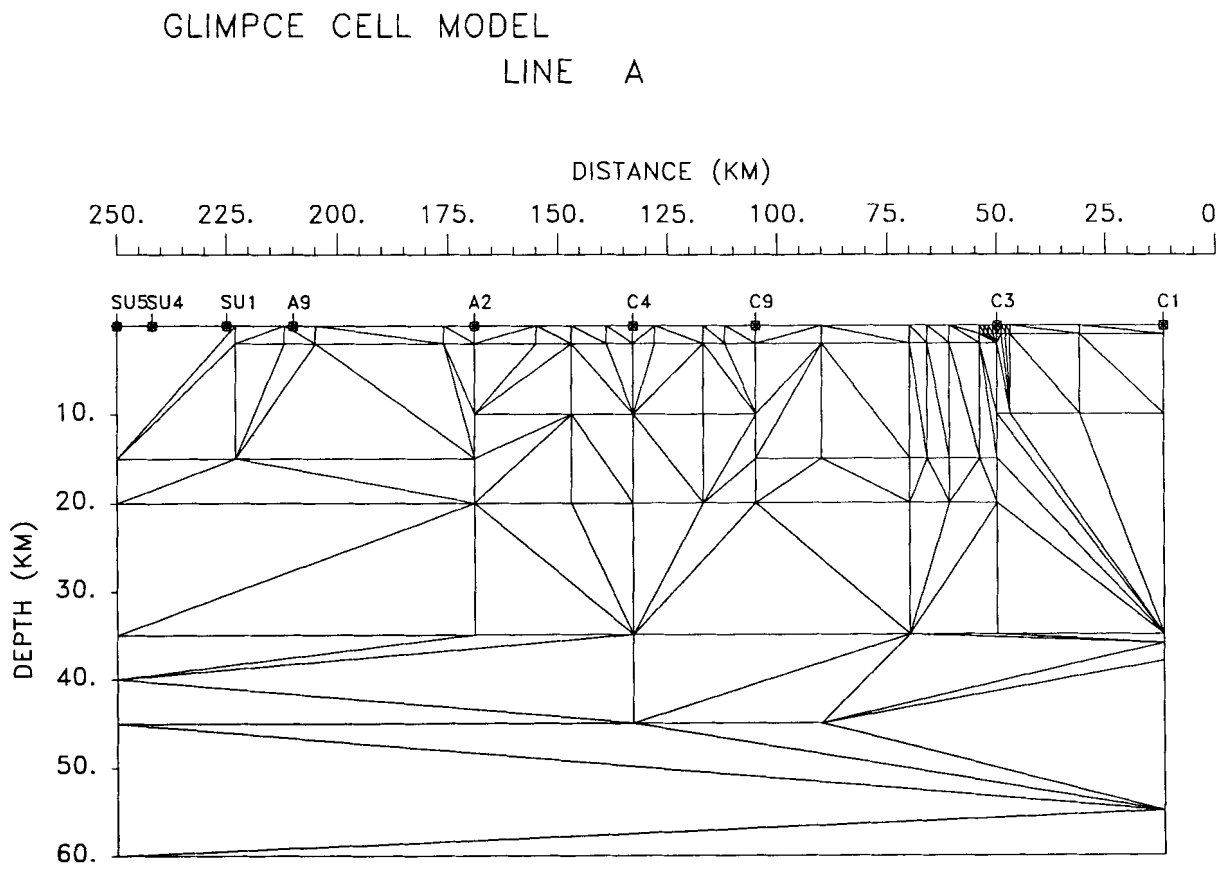

Figure 8. Cell configuration of the whole crust model. A total of 157 cells were used.

non-linearity in tomography, a slight change in any of the cell parameters could result in a dramatic change in the model traveltimes. A stable inversion method would constrain these changes, thereby yielding similar results for any given slight change in the initial conditions.

Initially, the cell model of Fig. 8 was superimposed on the whole crust model to determine qualitatively if the cell dimensions themselves had an adverse effect on the solution. No obvious connection between structure and cells was evident other than that of the sharp Moho boundaries, which was expected.

Next, each cell in the model was repeatedly subdivided into many more smaller cells in order to produce a fractal model. The manner in which this was done is illustrated by the simple triangle model given in Fig. 9(a), (b) and (c). In this example, each of the original four cells in the model (Fig. 9a) was subdivided into four new cells (Fig. 9b). Each of these 16 new cells was subdivided again by four, producing a 64-cell model. The process of subdivision continued and the result is a 256-cell fractal model (Fig. 9c). Thus, the fractal model is constructed by multiplying the cells in the original model by 4^n, where n is the number of subdivisions desired.

The whole crust velocity model (Fig. 7) contained 157 original cells, and each was subdivided into 64 new cells. Thus, the resulting fractal model consisted of 10,048 cells. Velocity gradients and horizontal and depth coordinates were recomputed for each of the new cells based on those values of the original model. A 2-D grid of smoothed random velocity perturbations was then superimposed on the model. These perturbations were no greater than 10 per cent of the model velocity. By ray tracing through this fractal velocity field and comparing the new model traveltimes with those obtained from the inversion, one can determine the stability of the technique itself. This method of measuring the effect of small velocity perturbations on a seismic model is based on the studies of Mereu & Ojo (1981) and of Ojo & Mereu (1985).

Traveltime comparisons for the observed, model and fractal model are presented in Fig. 10(a) for the C1 refraction and *PmP* data, and in Fig. 10(b) for the reverse-shot SU5 refraction and reflection data. Since both of these figures show how closely fitting the fractal times are to both the model and the observed times, we conclude that the model itself is reasonably stable. The small changes in the initial velocity field had very little effect on the final traveltimes, and there were only small differences in the velocity models.

DISCUSSION

Modelling results

There is no doubt that the method used for this work has yielded solutions that fit the observed data. This is clearly evident in the RMS–ray misfit values expressed in the traveltime comparison curves (Table 1); however, the reliability of this solution will depend on several other factors.

The first item to consider is the amount of *a priori* information available. In this work, the geology of the area

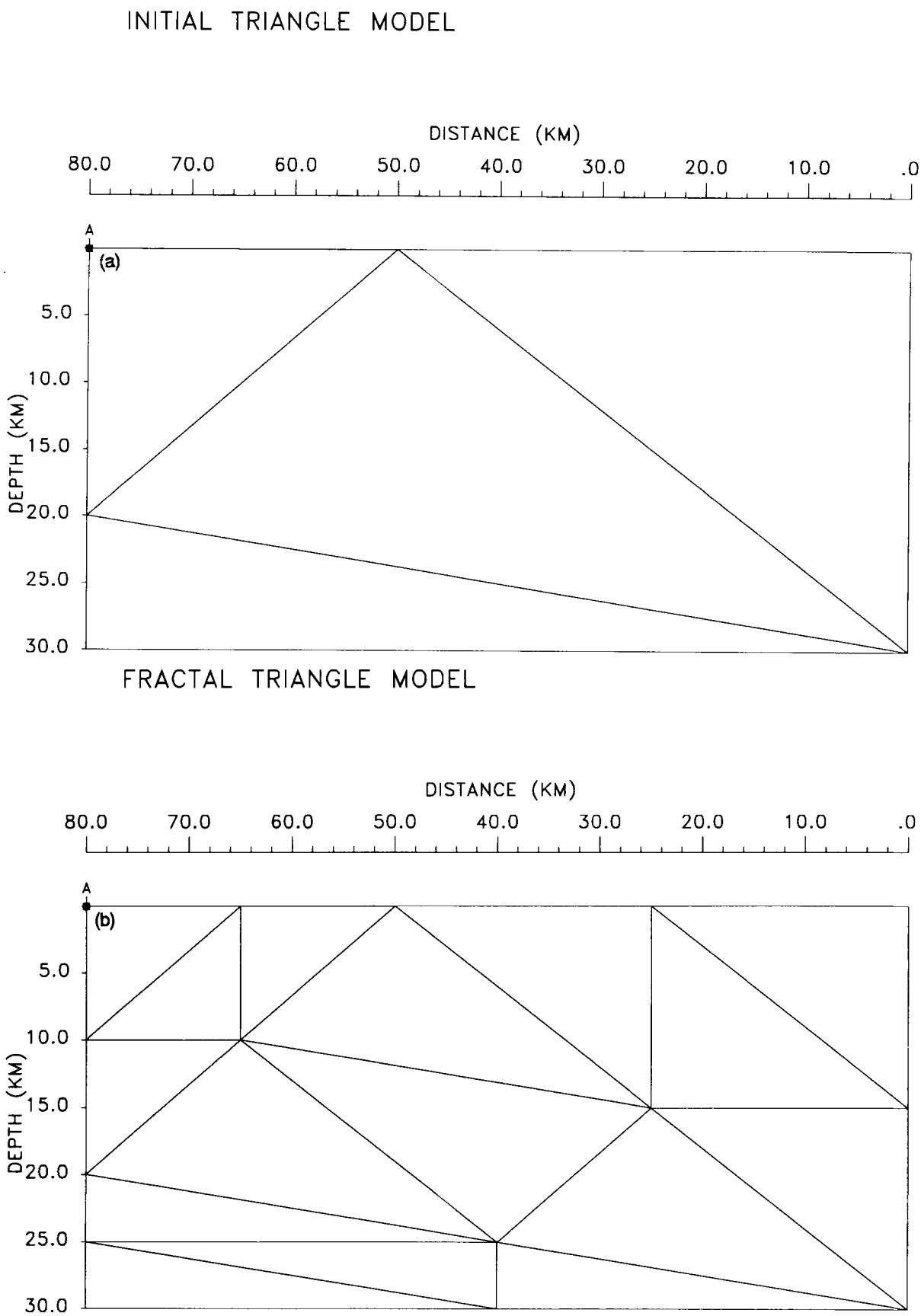

Figure 9. Fractal model stability test. Starting with an initial model (a), each cell is subdivided into four new cells with corresponding velocities (b). The process of cell subdivision is continued until the model is sufficiently 'fractal' (c) at which time ray tracing is performed and the fractal model times are compared with the initial and observed times.

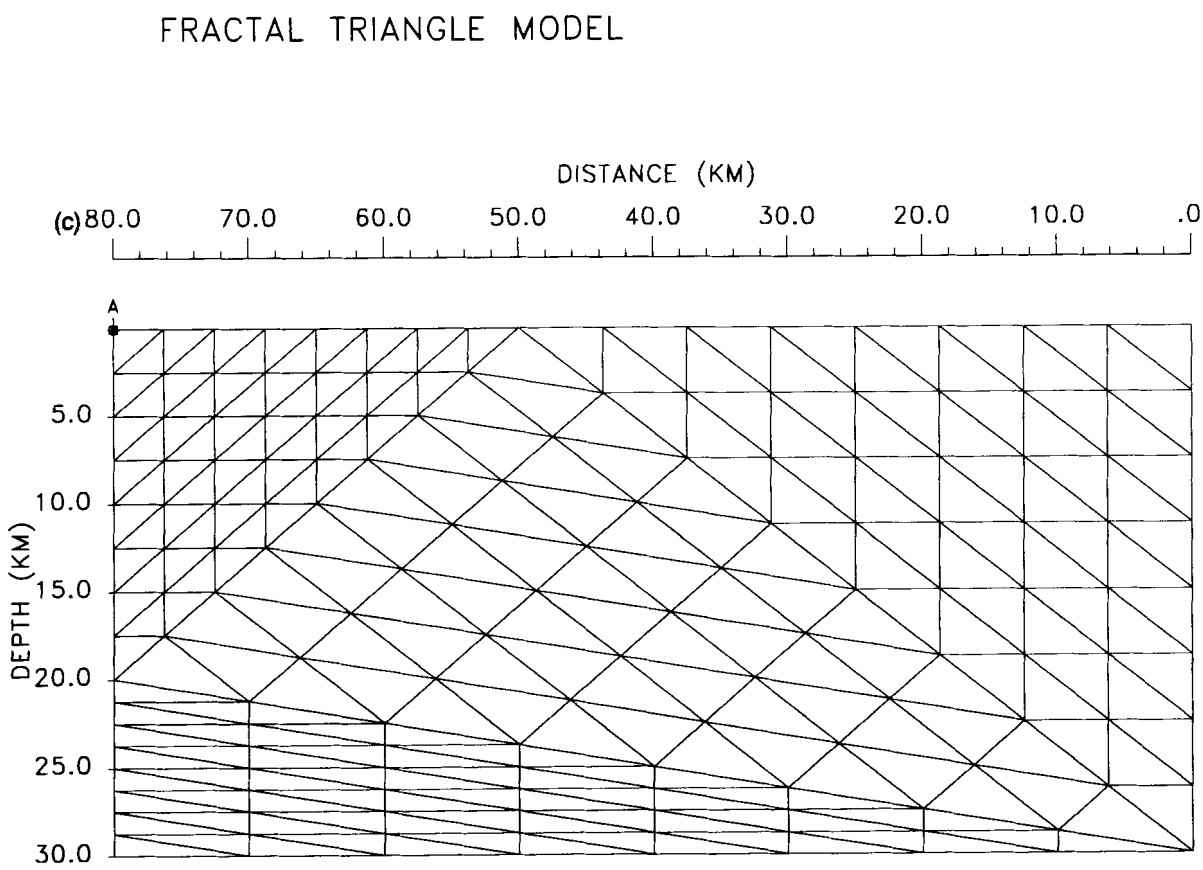

Figure 9 (c). (*Continued.*)

played an integral role, especially in the upper crust modelling. By incorporating such structures as low velocity sedimentary layers and higher velocity Pre-Cambrian Shield blocks into the model initialization, the non-uniqueness inherent in inverse problems can be fairly well constrained. This does not guarantee that the solution found will be the 'true' solution. All one can really hope for is that the solution is reasonable. Perhaps the best indication that this tomography method has produced just such a model is the result of the stability test.

A second factor to consider is how close the initial model is to the final model before inversion. During the course of this work, we found that if the initial model was too far out, then the algorithm had difficulty converging to a reasonable solution. As such, a trial and error method of determining initial model velocities by comparing roughly modelled and observed traveltimes before inversion is a good idea.

A third factor is the traveltime picking. In many cases, true *PmP* reflection signals from any given record are difficult to isolate, and this can lead to inversion of multiples or of noise. Solutions would be found, but they would be misleading if the wrong traveltime branch had been picked. As such, locating well defined observations and weighting them accordingly is very important in determining image reliability.

A fourth factor to consider is the number of cells that are used and the amount of crust that is to be imaged at any particular time. Since more geological information and good quality data were available in the upper crust, it was modelled first and then fixed before proceeding to greater depths. Any attempt to image the entire crust all at once with this type of surface-to-surface data set would probably lead to different results. By imaging the upper crust and fixing it, the deeper crust itself is better constrained and therefore less prone to unreliable results.

Finally, model resolution must be considered. White (1989) and White & Boland (1992) show that resolution at depth is generally very poor. Whereas our modelling technique tends to smooth features at depth into broader structures, the model of Tréhu *et al.* (1991) maintains rather unreasonably sharp boundaries. This is a result of the trial and error forward modelling method.

Geologic inferences

Seismic reflection analysis reveals the locations of the Keweenaw Fault zone (KF) near C3 and the Isle Royale Fault zone (IRF) near A2 (Cannon *et al.* 1989). These zones have been labelled in Fig. 7, but the refraction tomography method cannot resolve the actual fault boundaries. As such, these zones have been smoothed over.

The higher velocity (5.0–5.5 kms^{-1}) Superior Shoals (SS) have been resolved in the vicinity of A2–A9, whereas the lower velocity (4.0–4.5 kms^{-1}) KS layer extends over the rest of the lake area. We note that the KS layer decreases in thickness from approximately 5 km in the south to about 3 km near the SS and even less near the northern shoreline.

Of particular interest is the high velocity zone (7.0–7.2 kms^{-1}) at a depth of approximately 10 km underneath the C4 station. Apparently, the upper limit of

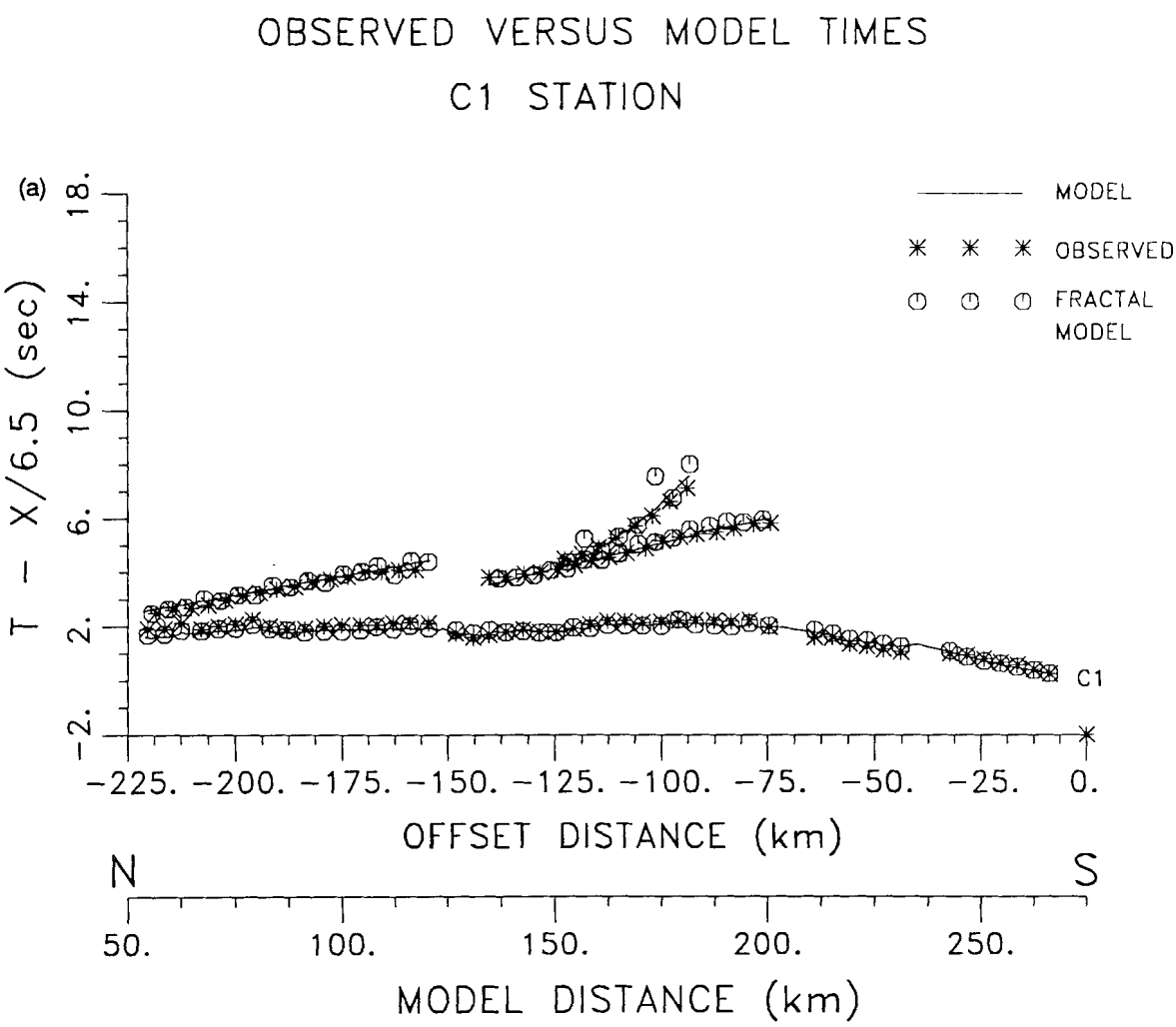

Figure 10. Comparisons of observed, whole model, and fractal model traveltimes for the C1 station (a) and for the SU5 station (b). The overall agreement of all times suggests that the whole model found in this work is stable and reasonable. Not all data have been plotted here for clarity.

the mantle intrusions has been resolved. This confirms the results of Behrendt *et al.* (1988); Cannon *et al.* (1989); the GLIMPCE Seismic Refraction Working Group (1989); Green *et al.* (1989), who suggest that the basaltic sequence contains velocities exceeding 7.0 kms^{-1} at relatively shallow depths (10–12 km) in the central basin.

The base of the high velocity intrusion is broad—at least 50 km wide under the CB. This is consistent with broad crustal swelling as described by Crough (1983); that is, thermal uplifting from a single crack in the crust does not appear to be a sufficiently realistic mechanism for this structure. Furthermore, previous models of this Lake Superior region indicate an intrusion base width of around 50 km (Gibson 1979; & Hinze *et al.* 1982), unlike the crack-and-flood model of Tréhu *et al.* (1991).

The block-like high-velocity structure under the NB (75 km, 30 km) is similar to that modelled by Tréhu *et al.* (1991). Because of the poor resolution at depth, it is difficult to determine if the origin of this structure is independent of the CB intrusion or not. The question of whether or not this feature may represent an earlier rifting episode cannot be answered by these findings.

CONCLUSIONS

The tomographic velocity model obtained from analysis of GLIMPCE Line A traveltime data indicates that the crust under Lake Superior is transitional and has been highly disrupted. This is consistent with the discontinuous Moho signals observed in the seismic records. The high velocity (7.0–7.2 kms^{-1}) intrusive zone under the central basin is composed of a broad-based mantle up-welling (approximately 50 km wide). A smaller intrusion is observed under the northern basin. Because of the poor resolution at depth, it is impossible to determine if these two intrusive blocks are independent or not. It is also difficult to ascertain whether or not these structures are distinct from one another.

The SVD routine used in the 2-D traveltime tomography inversion method proved to be practical and reliable. The stability test applied to the resulting velocity model proved that our model is also very stable. The tomography method itself reduces the subjectivity of trial and error forward modelling methods.

Although some questions persist regarding details of the complex nature of the North American MRS, the model

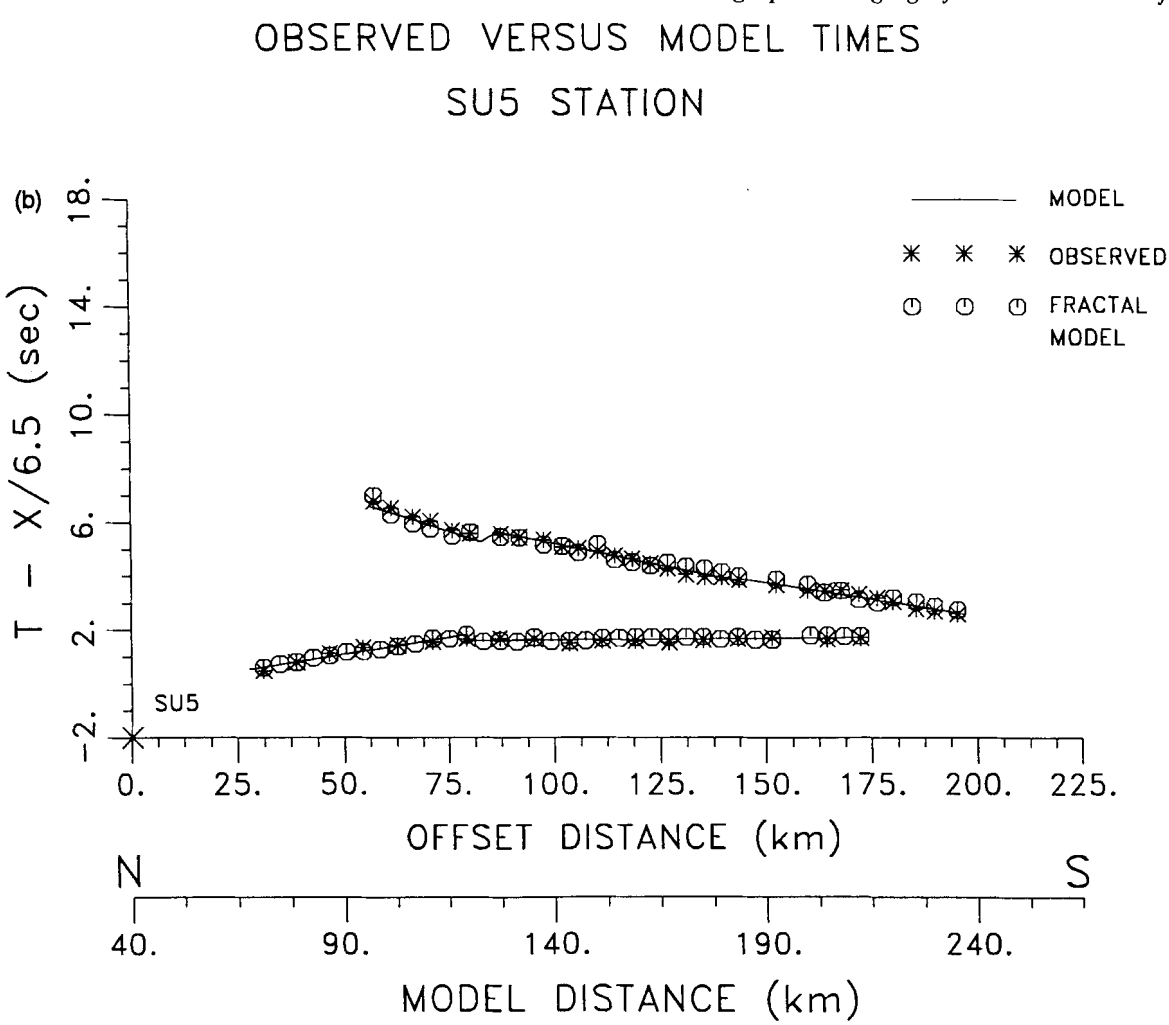

Figure 10 (b). (*Continued.*)

presented here adds further support to the theory that this Lake Superior structure is a failed rift zone.

ACKNOWLEDGMENTS

We would like to thank the organizers of the GLIMPCE seismic experiment for giving us the opportunity to participate in it. In particular, we acknowledge the Geological Survey of Canada and the United States Geological Survey. We would also like to thank Dr D. B. Snyder and an anonymous reviewer for their very helpful criticisms.

This research was supported by Natural Sciences and Engineering Research Council Grant No. A1793 and by an Energy Mines and Resources Grant No. 90 4 70. One of the authors (D. A. H.) was financially supported by two Canadian Society of Exploration Geophysicists scholarships, and by one Society of Professional Well Log Analysts scholarship.

REFERENCES

Aki, K., Christoffersson, A. & Husebye, E. S., 1977. Determination of the three-dimensional seismic structure of the lithosphere, *J. Geophys. Res.*, **82,** 277–296.

Beghoul, M. N., Hearn, T. M. & Barazangi, M., 1991. First tomographic study of western U.S. completed, *EOS, Trans. Am. geophys. Un.*, **71,** 1083.

Behrendt, J. C., Green, A. G., Cannon, W. F., Hutchinson, D. R., Lee, M. W., Milkereit, B., Agena, W. F. & Spencer, C., 1988. Crustal structure of the Mid-Continent Rift System: results from GLIMPCE deep seismic reflection profiles, *Geology,* **16,** 81.

Berry, M. J. & West, G. F. 1966. An interpretation of the first-arrival data of the Lake Superior Experiment by the time-term method, *Bull. seism. Soc. Am.*, **56,** 141–171.

Bishop, T. N., Bube, K. P., Cutler, R. T., Langan, R. T., Love, P. L., Resnick, J. R., Shuey, R. T., Spindler, D. A. & Wyld, H. W., 1985. Tomographic determination of velocity and depth in laterally varying media, *Geophysics,* **50,** 903–923.

Bording, R. P., Gersztenkorn, A., L. R., Scales, J. A. & Treitel, S., 1987. Applications of seismic traveltime tomography, *Geophys. J. R. astr. Soc.*, **90,** 285–303.

Bregman, N. D., Bailey, R. C. & Chapman, C. H., 1989. Crosshole seismic tomography, *Geophysics,* **54,** 200–215.

Cannon, W. F. & Davidson, D. M., Jr, 1982. Bedrock geologic map of the Lake Superior Region in *Geology and tectonics of the Lake Superior Basin,* pp. 280, eds Wold, R. J. & Hinze, W. J., Geological Society of America Memoir **156**.

Cannon, W. F., Green, A. G., Hutchinson, D. R., Lee, M. W., Milkereit, B., Behrendt, J. C., Halls, H. C., Green, J. C., Dickas, A. B., Morey, G. B., Sutcliffe, R. & Spencer, C.,

1989. The Midcontinent Rift beneath Lake Superior from GLIMPCE seismic reflection profiling, *Tectonics*, **8,** 305.

Crough, S. T., 1983. Rifts and swells: geophysical constraints on causality, *Tectonophysics*, **94,** 23–37.

Dines, K. & Lytle, R. J., 1979. Computerized geophysical tomography, *Proc. IEEE*, **67,** 1067–1073.

Dziewonski, A. M. & Anderson, D. L., 1984. Seismic tomography of the Earth's interior, *Am. J. Sci.*, **72,** 483–494.

Epili, D. & Mereu, R. F., 1989. The GLIMPCE seismic experiment: onshore refraction and wide-angle reflection observations from a fan line over the Lake Superior Midcontinent Rift System, in Properties and Processes of Earth's Lower Crust, *Geophys. Monogr. IUGG Ser.* 6, **51,** 93–101.

Epili, D. & Mereu, R. F., 1991. The Grenville Front Tectonic Zone: results from the 1986 Great Lakes onshore seismic wide-angle reflection and refraction experiment, *J. Geophys. Res.*, **96,** 16,335–16,348.

Gibson, J. D., 1979. Gravity and magnetic modelling in the Lake Superior region, *Senior Honours Project,* Purdue University, USA.

GLIMPCE Seismic Refraction Working Group., 1989. GLIMPCE seismic experiments: long offset recordings, *EOS, Trans. Am. geophys. Un.*, **70,** 841, 852–853.

Green, A. G., Cannon, W. F., Milkereit, B., Hutchinson, D. R., Davidson, A., Behrendt, J. C., Spencer, C., Lee, M. W., Morel-à-l'Huissier, P. & Agena, W. F., 1989. A 'GLIMPCE' of the deep crust beneath the Great Lakes, in *Properties and Processes of Earth's Lower Crust,* pp. 65–80, ed. Mereu, R. F., Mueller, St. & Fountain, D., *Geophys. Monogr., IUGG Ser.* 6, **51,** AGU, Washington, DC.

Hamilton, D. A., 1991. Two-dimensional tomographical tweaking of the GLIMPCE data set across the Midcontinent Rift Zone, *MSc. thesis,* University of Western Ontario, Canada.

Hinze, W. J. & Wold, R. J., 1982. Lake Superior geology and tectonics—overview and major unresolved problems in *Geology and tectonics of the Lake Superior Basin,* pp. 273–280, eds Wold, R. J. & Hinze, W. J., Geol. Soc. Am. Memoir, **156.**

Hinze, W. J., Wold, R. J. & O'Hara, N. W. 1982. Gravity and magnetic anomaly studies of Lake Superior, in *Geology and tectonics of the Lake Superior Basin,* pp. 203–221, eds Wold, R. J. & Hinze, W. J., Geol. Soc. Am. Memoir, **156.**

Klasner, J. S., Cannon, W. F. & Van Schmus, W. R. 1982. The pre-Keweenawan tectonic history of southern Canadian Shield and its influence on formation of the Midcontinent Rift, in *Geology and tectonics of the Lake Superior Basin,* pp. 27–46, eds Wold, R. J. & Hinze, W. J., Geological Society of America Memoir, **156.**

Luetgert, J. H. & Meyer, B. P., 1982. Structure of the western basin of Lake Superior from cross structure refraction profiles in *Geology and tectonics of the Lake Superior Basin,* pp. 245–256, eds Wold, R. J. & Hinze, W. J., Geol. Soc. Am. Memoir, **156.**

Mereu, R. F., 1990. An interpretation of CCSS data set I using the triangular block model method, in *Studies of laterally heterogeneous structures using seismic refraction and reflection data,* ed. Green, A. G., Geological Survey of Canada, Paper 89–13, pp. 53–63.

Mereu, R. F. & Ojo, S. B., 1981. The scattering of seismic waves through a crust and upper mantle with random lateral and vertical inhomogeneities, *Phys. Earth planet. Interiors,* **26,** 233–240.

Morel-à-l'Huissier, P., Karl, J. H., Tréhu, A., Hajnal, Z., Mereu, R. F., Meyer, R. P., Sexton, J. L., Erwin, G. P., Green, A. G. & Hutchinson, D., 1990. The 1986 Great Lakes refraction survey (GLIMPCE): Line A—refraction mode, *Geol. Surv. Can.* (open file report 2283).

Nolet, G., 1987. *Seismic Tomography with Applications in Global Seismology and Exploration Geophysics,* Reidel, Dordrecht.

Ojo, S. B. & Mereu, R. F., 1985. The effect of random velocity functions on the traveltimes and amplitudes of seismic waves, *Geophys. J. R. astr. Soc.*, **84,** 607–618.

Peterson, J. E., Paulson, B. N. P. & McEvilly, T. V., 1985. Applications of algebraic reconstruction techniques to cross-hole seismic data, *Geophysics*, **50,** 1566–1580.

Press, W. H., Flannery, B. P., Teukolsky, S. A. & Vetterling, W. T., 1986. *Numerical Recipes,* Cambridge University Press, Cambridge.

Scales, J. A., 1987. Tomographic inversion via the conjugate gradient method, *Geophysics,* **52,** 179–185.

Steinhart, J. S. & Smith, T. J., 1966. *The Earth Beneath the Continents,* Geophys. Monogr. Ser., **10,** 663, AGU, Washington, DC.

Tréhu, A., Morel-à-l'Huissier, P., Meyer, R., Hajnal, Z., Karl, J., Mereu, R., Sexton, J., Shay, J., Chan, W.-K., Epili, D., Jefferson, T., Shih, X.-R., Wendling, S., Milkereit, B., Green, A. & Hutchinson, D., 1991. Imaging the midcontinent rift beneath Lake Superior using large aperture seismic data, *Geophys. Res. Lett.*, **18,** 625–628.

Van Schmus, W. R. & Hinze, W. J., 1985. The Mid-continent Rift System, *Ann. Rev. Earth planet. Sci.*, **13,** 345.

White, D. J., 1989. Two-dimensional seismic refraction tomography, *Geophys. J.*, **97,** 223–245.

White, D. J. & Boland, A. V., 1992. A comparison of forward modeling and inversion of seismic first arrivals over the Kapuskasing Uplift, *Bull. seism. Soc. Am.*, **82,** 304–322.